Absolute high-resolution rate coefficients for dissociative recombination of electrons with HD^+: Comparison of results from three heavy-ion storage rings

A. Al-Khalili,[1,2] S. Rosén,[1] H. Danared,[3] A. M. Derkatch,[1] A. Källberg,[3] M. Larsson,[1] A. Le Padellec,[1,4] A. Neau,[1] J. Semaniak,[2] R. Thomas,[1,5] M. af Ugglas,[3] L. Vikor,[1] W. Zong,[1] W. J. van der Zande,[5,*] X. Urbain,[6,†] M. J. Jensen,[6] R. C. Bilodeau,[6] O. Heber,[7] H. B. Pedersen,[6] C. P. Safvan,[6] L. H. Andersen,[6] M. Lange,[8,‡] J. Levin,[8] G. Gwinner,[8] L. Knoll,[8] M. Scheffel,[8] D. Schwalm,[8] R. Wester,[8] D. Zajfman,[7,8] and A. Wolf[8]

[1]*Department of Physics, Stockholm University, SCFAB, S-106 91 Stockholm, Sweden*

[2]*Institute of Physics, Swietokzryska Academy, 25 406 Kielce, Poland*

[3]*Manne Siegbahn Laboratory, Stockholm University, S-104 05 Stockholm, Sweden*

[4]*LCAR UMR 5589, Université Paul Sabatier–Toulouse III, 118 route de Narbonne, Batîment III R1B4, 31062 Toulouse Cedex 4, France*

[5]*FOM-Institute AMOLF, Kruislaan 407, 1098 SJ Amsterdam, The Netherlands*

[6]*Department of Physics and Astronomy, University of Aarhus, DK-8000 Århus C, Denmark*

[7]*Department of Particle Physics, Weizmann Institute of Science, 76100 Rehovot, Israel*

[8]*Max-Planck-Institut für Kernphysik, 69117 Heidelberg, Germany*

(Received 16 April 2003; published 6 October 2003)

Experimental data are presented from three different heavy-ion storage rings (ASTRID in Aarhus, CRYRING in Stockholm, and TSR in Heidelberg) to assess the reliability of this experimental tool for the extraction of absolute rate coefficients and cross sections for dissociative recombination (DR). The DR reaction between HD^+ and electrons has been studied between 0 and 30 eV on a dense energy grid. HD^+ displays two characteristic local maxima in the DR rate around 9 and 16 eV. These maxima influence the data analysis at smaller collision energies. We conclude that resonant structures in the DR cross sections are reproduced among the experiments within the collision energy resolution. The absolute cross sections agree within the systematic experimental errors of 20% related to the measurement of the ion currents. Absolute thermal rate coefficients for HD^+ ions are given for an electron temperature range of 50–300 K. Results for the DR cross section and the thermal rate coefficients are compared to recent theoretical calculations including rotational effects, finding satisfactory agreement.

DOI: 10.1103/PhysRevA.68.042702 PACS number(s): 34.80.Lx

I. INTRODUCTION

Dissociative recombination (DR) has been a subject of research for more than 50 years [1] now. In a DR event, a molecular ion captures an electron (with energy E) forming an intermediate doubly excited neutral molecule that rapidly dissociates into (possibly excited) fragments; for a diatomic molecule, $AB^+ + e^-(E) \rightarrow AB^{**} \rightarrow A^* + B^* + E_k$. The symbol E_k stands for the kinetic-energy release (KER) given to the fragments. The total energy set free by the dissociation is shared between the excitation energy of the fragments and their kinetic energy.

DR is an important process in low-temperature astrophysical plasmas. In particular, in interstellar clouds many molecules are formed by reactions involving molecular ions, and a good understanding of the DR process is required to predict the abundance of many molecular species in this environment [2]. In planetary atmospheres, DR is a sink of thermal electrons and the large exothermicity of the DR reaction with molecular nitrogen [3] is responsible for escape of nitrogen atoms from Mars; DR also leads to airglows in the terrestrial atmosphere such as, for O_2^+, by the subsequent $O(^1S)$ green light emission [4,5].

DR of molecular hydrogen serves as the prototypical DR reaction. In spite of its apparent simplicity, being a one-electron system, DR of H_2^+ is theoretically challenging. Although theory is making progress [6–8], it cannot yet be used as an *a priori* reliable standard.

Experimental research on DR initially used stationary afterglow techniques [9]. Later, flowing-afterglow instruments [10], crossed beams [11], and single-pass merged beams arrangements [12] have been employed. The first DR signal from molecular ions at a heavy-ion storage ring was reported for H_2^+ ions at the TARN II facility in Tokyo in 1991 [13]. The suggestion to use a heavy-ion storage ring as a multiple-pass merged beams setup and to employ the cooling of internal degrees of freedom by radiative emission during the beam storage was also put forward in 1992 by Datz and Larsson [14] in a discussion of HeH^+. These preliminary studies were followed by initial storage-ring experiments dedicated to molecular recombination [15–17] and an intensive molecular DR program in four heavy-ion storage-ring facilities. The rings are ASTRID [18] in Aarhus, CRYRING [19] in Stockholm, TARN II [13] in Tokyo, and TSR [20] in Heidelberg. All four setups have been able to determine absolute DR cross sections and rate coefficients for vibra-

*Present address: Department of Molecular and Laser Physics, University of Nijmegen, Nijmegen, The Netherlands.

†Permanent address: Département de Physique, Université Catholique de Louvain, Louvain-la-Neuve, Belgium.

‡Present address: Atomic and Molecular Physics Laboratories, Research School of Physical Sciences and Engineering, Australian National University, Canberra, Australia.

 ©2003 The American Physical Society

tionally cold species. At present, the heavy-ion storage-ring technique also provides the internal state distributions of the fragments or, in the case of molecular fragments from the DR of polyatomic molecular ions, the branching ratios for the different product channels.

Among the numerous species studied so far, the molecular ions H_2^+, H_3^+, and HeH^+ and their isotopomers have been studied in most detail. Peart and Dolder [21] performed the first ion-beam experiments. Phaneuf *et al.* [22] measured partial cross sections. McGowan and co-workers have studied H_2^+ using a high-resolution merged beams set-up [12]. These authors recognized that the vibrational population in the H_2^+ ion beam affects the DR yield. They devised methods to quench the vibrational excitation prior to acceleration of the ions [23,24]. Since storage rings can routinely store ions for periods of many seconds, those molecular ions that are infrared active, such as HD^+, the subject of this paper, will lose rovibrational excitation energy by emission of radiation.

In 1993, the first measurement of the (relative) cross section for the DR of HD^+ in a heavy-ion storage ring was performed at TSR [16,25]. Experiments following that concentrated on the local maximum in the cross section at $E \sim 9$ eV and on the effects of the different isotopomers of hydrogen [6,7,26]. The excellent collision energy resolution of the storage rings was exploited in studies of the resonance structure at low ($E<0.1$ eV) collision energy [27,28]. The sensitivity of these instruments was used for a detailed study near the minimum of the cross section around $E=1$ eV [29]. Experiments have addressed directly and indirectly the vibrational state dependence of the DR cross sections. In ASTRID, photodissociation of H_2^+ has been used to modify the vibrational population, and clear indications were found of a strong dependence of the DR rates on the vibrational state [26,30]. At CRYRING, observations of time-dependent DR rates during rovibrational relaxation of the ions have been interpreted qualitatively in terms of state-specific cross sections [31]. At TSR, the Coulomb explosion imaging technique provides a direct access to the vibrational population of the ion beam, and vibrational state-specific cross sections were reported on HD^+ [32,33].

DR of HD^+ is an ideal benchmark system for absolute-cross-section measurements. HD^+ displays a highly structured cross section, which can be used to trace differences in the collision energy scale determination. The vibrational modes of HD^+ are infrared active, and full vibrational cooling down to room temperature, with negligible population in excited vibrational states, is achieved in less than 1 s. This relaxation of the ions prevents differences in the acquired data that could arise from the different ion sources used in each of the rings. Even rotational relaxation takes place to a large extent within the used storage times; the decay time is shorter than 1.6 s for all rotational levels $J>3$ [34]. The absence of radiative decay channels excludes H_2^+ as a simple benchmark system, since the internal state of the H_2^+ ions would then be dependent on the local ion source conditions. However, it has been shown recently that vibrational relaxation does occur through superelastic collisions with the electrons in the electron target [35].

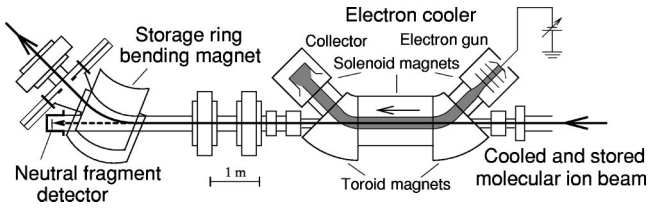

FIG. 1. Schematic layout of the merged beams arrangement used for electron-ion recombination measurements at ion storage rings, showing the electron cooling device, magnetic elements of the storage ring, and the location of the neutral fragment detectors for the Heidelberg heavy-ion storage-ring TSR.

In this paper, we present a comparative study performed at three ion-storage rings. Since the experimental parameters and procedures at the three setups differ in many details, the reliability of the storage-ring technique in producing absolute cross sections and energy dependences for the DR of molecular ions can be verified. Uncertainties in the initial conditions are largely eliminated through the efficient radiative cooling of the HD^+ ions. Moreover, consolidated DR data for the hydrogen molecular ion and its isotopomers are of particular interest for benchmark comparisons with existing and future theoretical calculations.

In the following, the experimental procedures applied at the various storage rings are described. Then the absolute cross section data from the different experiments are compared with each other. The extraction of thermal rate coefficients for the low-energy DR is discussed and joint results are given where possible. We conclude with a comparison against previously published results and recent theoretical calculations.

II. EXPERIMENT

A. General aspects

Three ion storage rings participated in the present comparison by performing dedicated measurements; ASTRID at Aarhus University (Aarhus, Denmark), CRYRING at the Manne Siegbahn Laboratory (Stockholm, Sweden), and TSR at the Max-Planck-Institut für Kernphysik (Heidelberg, Germany). As an example, the configuration and dimensions of TSR are given in Fig. 1. The scale and layout of all three rings, storing the ions at MeV energies, are comparable in spite of several differences (see Table I). In all three rings, ions are created in an external ion source and, after extraction, transported into the ring through a magnetic beam line. At TSR, the ions are accelerated to the final energy prior to injection into the main ring, which enables the measurements to start as soon as the beam orbit is stabilized (~ 1 ms). At ASTRID and CRYRING acceleration takes place after injection, using a radio-frequency field. The stored ions merge in one section of the ring with an intense monoenergetic electron-beam, which is much wider than the ion beam and guided by a longitudinal magnetic field. The electron beam device is called the electron cooler. At the two ends of the electron cooler, where the beams merge and separate, the electron beam is deflected in toroidal magnetic sections with radius r_t, directly connected to both ends of a straight

TABLE I. Parameters for the HD^+ DR measurements at the three ion storage-ring facilities.

Item	Symbol	ASTRID	CRYRING	TSR	Unit
Ring circumference	C	40.0	51.7	55.4	m
Ion-beam energy	E_i	3.0	3.0	2.0	MeV
Ion-beam 1/e lifetime		7.5	6.5	24	s
Measurement time interval[a]		8–15	5–8	10–15	s
Detector size		6[b]	6[b]	4 (6)[c]	cm
Detector distance[d]		7	4	6.5	m
Electron thermal energy	$kT_{e\perp}$	22	2	4.5 (28)[e]	meV
Electron density[f]	n_e	4.1	5.6	2.6 (19)[e]	10^6 cm^{-3}
Electron-beam radius	a	10.6	20	25 (9.5)[e]	mm
Solenoid length	L_{sol}	1.0	1.10	1.50	m
Toroid bending radius	r_t	0.4	0.41	0.8	m
Electron guiding magnetic-field strength[g]		36	30	21	mT
Storage-ring dipole magnetic field strength		0.38	0.40	0.31	T
Field ionization limit[h]	n_c	9	9	10	

[a]Time after injection.
[b]Radius.
[c]Vertical (horizontal) dimensions.
[d]From center of electron cooler (approximate).
[e]Wide-beam (narrow-beam) settings (see Sec. II C 3).
[f]At the cooling energy ($E_d=0$; see Sec. II A).
[g]Longitudinal magnetic field present in the interaction region.
[h]Critical quantum number n_c (see Sec. II B).

magnetic-field section produced by a solenoid of length L_{sol}. The geometrical parameters are different for the three rings as listed in Table I.

The electrostatic interaction between electrons and ions results in phase-space cooling of the ion beam [36] at the expense of the very low temperature of the continuously renewed electron beam. The electron cooler also serves as an electron target for the DR experiments. When the mean velocity of the electrons is equal to that of the ions, near-zero collision energies are obtained. The typical ion-beam diameter after phase-space cooling is <2 mm, much smaller than the electron-beam radius in the various setups (Table I). The cooling energy at the center of the electron beam is easily found by optimizing the strength of the DR signal itself, since the DR cross section increases strongly towards zero collision energy. By tuning the velocity of the electrons away from the ''cooling'' velocity, DR can be studied at very well controlled collision energies over a wide range of energies. The electrons can be both accelerated and decelerated with respect to the ion beam, to achieve the same center-of-mass collision energy.

At a given setting of the electron acceleration voltage, the average velocity of the electrons with respect to that of the ions is directed longitudinally, along the direction of the two beams (assumed to be collinear), and is denoted by the ''detuning'' velocity v_d. From this velocity the 'detuning energy' $E_d=(m/2)v_d^2$ is calculated (where m is the electron mass); v_d and E_d are in fact controlled by the acceleration voltage of the electron beam (the ion-beam velocity remaining fixed). The electron energies E for individual collisions show a statistical scatter with values close to E_d, and their distribution follows from that of the relative electron-ion velocities $\vec{v}$. The distribution of the relative velocities has been found [37–39] to be well represented by the anisotropic Maxwellian

$$f(v_d,\vec{v})=\frac{m}{2\pi kT_\perp}\sqrt{\frac{m}{2\pi kT_\parallel}}\exp\left[-\frac{mv_\perp^2}{2kT_\perp}-\frac{m(v_\parallel-v_d)^2}{2kT_\parallel}\right], \tag{1}$$

where $v_\perp$ and $v_\parallel$ denote the transversal and longitudinal components, respectively, of the relative velocity $\vec{v}$ and $T_\perp$ and $T_\parallel$ are the temperatures associated to the relative motion in the respective degrees of freedom. As the ion beam is phase-space cooled, the dominant velocity spread regarding the relative motion is that of the electrons (as characterized by the temperatures $T_{e\perp}$ and $T_{e\parallel}$ of the electron beam in its comoving reference frame); hence, $T_\perp\sim T_{e\perp}$ and $T_\parallel\sim T_{e\parallel}$. The electron temperatures in the transversal and longitudinal degrees of freedom are decoupled by the guiding magnetic field of the electron-beam (see Table I). The longitudinal electron temperature is strongly reduced as compared to the cathode temperature (~ 0.1 eV/k for the thermionic cathodes used here) by the spatial expansion of the electron ensemble that takes place during the electron-beam acceleration, reaching beam energies of ~ 550 eV for ASTRID and CRYRING and ~ 360 eV for TSR. This kinematical effect due to the acceleration is partly counteracted by electron-electron interactions [40]; the resulting longitudinal electron temperature typically amounts to $kT_{e\parallel}\sim 1\times 10^{-4}$ eV. The transverse electron temperature can be reduced with respect to the cathode temperature through an adiabatic magnetic expansion

[41,42] of the electron-beam. The electron beam devices employed at the three storage rings use different magnetic expansion factors yielding the transverse electron temperatures listed in Table I.

The validity of Eq. (1), with typically $T_{\parallel} \ll T_{\perp}$, was verified experimentally in a single-pass experiment merged beams experiment by the Aarhus group [37] and by later storage-ring experiments [38,39], using narrow recombination resonances of atomic ions. The velocity distribution $f(v_d, \vec{v})$ of Eq. (1) generally leads to an asymmetric broadening of a sharp resonance in the observed energy dependent cross section, a resonance at $E_{d,r}$ being broadened by $kT_{\perp}$ towards the low-energy side ($E_d < E_{d,r}$) and, in addition, symmetrically with a width [full width at half-maximum (FWHM)] of $4(E_d kT_{\parallel} \ln 2)^{1/2}$ around $E_{d,r}$ [37,43]. As the broadening effect of the longitudinal temperature scales as $\propto E_d^{1/2}$, it dominates the observed resonance shape at energies above the limit $E_d \gtrsim kT_{\perp}^2/2T_{\parallel}$. This yields, for example, at CRYRING (see Table I) FWHM energy resolutions of $\sim$10 meV and $\sim$33 meV for $E_d = 0.1$ eV and 1 eV, respectively, while a resolution down to the transverse thermal energy of $kT_{\perp} = 2$ meV is achieved only for $E_d \lesssim 0.02$ eV.

The neutral DR fragments do not follow the ions in the first dipole bending magnet after the electron cooler and are monitored by detectors located on a parallel line drawn from the axis of the electron cooler. The KER given to the fragments causes them to be slightly scattered away from the axis of the ion beam through the cooler, and the size of the detectors has been chosen such that all fragments are detected. The high energy of the ion beam makes it possible to have unity detection efficiency with solid-state detectors. Furthermore, the resolving power of the solid-state detectors makes it possible to distinguish DR events (depositing the full beam energy of the HD^+ ions for each event) from the most prominent form of background. These background processes produce H or D atoms (plus undetected ionic fragments) through the destruction of the HD^+ ions in collisions with residual-gas and, at higher electron collision energies, via electron-induced dissociative processes (dissociative excitation). Typical residual gas pressures in the rings are in the 10^{-11} mbars range (mainly H_2). The detector signals at 1/3 or 2/3 of the beam energy yield reference count rates (denoted by R_H and R_D, respectively) which allow the DR counts to be normalized to the instantaneous relative ion current. Absolute measurements require in addition a calibration of the reference count rate versus the absolute ion current.

B. Experimental details

The three experiments differ in the details of their procedure and data analysis. The general character of the procedures and some of their common aspects are discussed in the following.

(a) Variation of the electron collision energy and normalization of the signals to obtain absolute cross sections and rate coefficients. The experiments at ASTRID and TSR use sudden changes in the electron beam energy, the so-called jump method, whereas, in CRYRING, the electron beam energy was slowly and continuously ramped up and down, the so-called ramp method. Both types of energy variations have proven to be well suited for high-resolution experiments on electron-ion interaction [43,44] and primarily differ in technical aspects. In all three rings, the relative cross sections are obtained by normalizing to some reference, either the background count rates R_H or R_D or the signal count rate at the cooling voltage. The absolute-cross-section determination requires a calibration through a simultaneous measurement of the respective reference count rate and the ion current. During the DR measurement the ion current must be kept at $\sim$10–100 nA as otherwise large DR count rates would cause damage to the particle detectors. On the other hand, the nondestructive ion current measuring devices available at TSR and CRYRING typically operate in current ranges of μA. Therefore, the calibration at these facilities was performed in two steps either by an intermediate signal (Sec. II C 3) or by time extrapolation (Sec. II C 2). At ASTRID (ion current sensitivity down to 50 nA) DR and ion current signals were directly available at the same time. In all experiments the constancy of the residual-gas pressure was verified by vacuum measurements; the calibrations of the reference count rates were repeated at different times. The ion current calibration introduces the largest systematic error to the absolute-cross-section scale, which is estimated to be $\pm 20\%$ at all three facilities.

Contaminations of the stored HD^+ beam by isobaric H_3^+ ions were avoided at CRYRING and TSR by producing the ions from HD gas in electron-impact ion sources. At ASTRID a mixture of H_2 and D_2 gas was used in the ion source, and its operating conditions were chosen such that no significant production of D_3^+ was observed. The absence of an H_3^+ contamination in the stored beam was verified experimentally at CRYRING [28] using a combination of grids and absorbers installed in front of the solid-state detector. At TSR, the Coulomb explosion imaging technique used in vibrational state-specific cross-section measurements [32,33] is sensitive to H_3^+ contaminations but none were observed. From these findings and diagnostic measurements any H_3^+ contaminations are estimated to be below the percent level.

(b) Results for the experimental cross section. For background-subtracted count rates $\overline{R}_{H+D}$ of recombination events with their associated values of the ion current I_i and the electron density n_e, as determined for all detuning energies E_d, the experimental recombination rate coefficient α is obtained on an absolute scale as

$$\alpha(E_d) = \langle \sigma v \rangle = \frac{\overline{R}_{H+D}}{N_i n_e} = \frac{e v_i}{L I_i n_e} \overline{R}_{H+D}, \tag{2}$$

where, in addition, v_i denotes the (fixed) ion-beam velocity and N_i denotes the number of ions in the interaction region of length L [see remarks on L following Eq. (5)]. No detector efficiency factor is used as the geometric and electronic inefficiencies of the detection system are estimated to be negligible within the overall absolute calibration error of $\pm 20\%$. The angular brackets indicate the averaging over the experimental electron velocity distribution inherent to the experimental procedure. The rate coefficient is measured as a

function of the detuning energy E_d ranging from $\sim 10^{-4}$ eV up to ~ 30 eV. Over most of this range E_d largely exceeds the thermal velocity spread of the electron beam and hence the electron energies are distributed in a narrow band close to E_d. It is therefore reasonable to derive the absolute experimental cross section as $\langle \sigma v \rangle / v_d$, dividing the observed absolute rate coefficient through the detuning velocity. Narrow structures in the true cross section appear folded with the effective collision energy resolution in this experimental cross section. Only at small detuning velocities, if the collision energies approach the temperature of the electron beam, do larger differences between the experimental values and the true cross sections become noticeable. No deconvolution procedures have been applied in this paper.

(c) Determination of the absolute collision energy scale. The detuning energy E_d follows [43] from the laboratory energies of the electron and ion beams, E_e and E_i. The laboratory electron energy E_e varies with the radial distance from the center of the electron beam due to electron space charge. Hence, E_e is obtained from the electron acceleration voltage including a space-charge correction [43]. The energy E_i of the ions is monitored by measuring their revolution frequency in the storage ring, yielding relative and absolute accuracies of $\sim 10^{-4}$ and $\sim 10^{-3}$, respectively. The zero point of E_d can be fixed within $<10^{-4}$ eV by finding the cooling energy, as discussed in Sec. II A.

The measurement of the revolution frequency of the cooled ion beam is also used for centering the ion beam inside the electron beam (typically to within 2 mm), varying the lateral displacement between the electron and the ion beam until the local electron energy seen by the ions, as influenced by the electron space charge, and hence the ion revolution frequency assume a minimum. While the total space-charge *shift* of the electron energy is significant, the collision energy *spread* introduced by the space-charge profile of the electron beam remains small compared to the thermal broadening discussed following Eq. (1), owing to the small size of the cooled ion beam. The estimated space-charge effect on the collision energy (scaling as $\propto E_d^{1/2}$) for radial shifts of <2 mm is <10 meV at the typical electron density (10^7 cm^{-3}) and at $E_d = 1$ eV; this is small in comparison with the thermal broadening estimated in Sec. II A.

Partial compensation of the electron space charge may occur by trapped residual-gas ions, which can affect the accuracy of the energy scale for larger detuning E_d. In CRYRING a semiempirical formula is employed for this correction, whereas in TSR and ASTRID clearing electrodes prevent accumulation of thermal positive ions at the center of the electron beam so that the full space charge can be assumed when finding E_e.

(d) Correction for the bending regions of the electron beam at the beginning and the end of the interaction region. In the regions of the electron cooler where the ion and electron beams merge and separate (see Sec. II A) the angle between the beams differs from zero and with increasing angle the collision energy between the ions and the electrons increases rapidly [45]. Hence, at each detuning energy E_d as set by the electron acceleration voltage, the DR signal samples also the cross section for detuning energies $\tilde{E}_d$ larger than E_d. As the DR signal is evaluated according to Eq. (2) with the straight beam overlap length L, neglecting the bends, these contributions with $\tilde{E}_d > E_d$ add to the measured rate coefficient. In particular, the presence of a strong feature in the cross section at high collision energy, as found for the DR of HD^+ and many other species, has a significant effect on the observed cross section at lower energies. These contributions are modeled by describing the detuning energy in the bent regions by a function $\tilde{E}_d(x, E_d)$ where x denotes the longitudinal position along the ion beam. The function $\tilde{E}_d(x, E_d)$ is essentially determined by the angle $\theta(x)$ between the electron and the ion beam and the laboratory velocities v_e and v_i of the two beams according to

$$\tilde{E}_d(x, E_d) = E_d + m v_i v_e [1 - \cos\theta(x)]. \tag{3}$$

Setting $x = 0$ at the mechanical connection between the solenoid and the toroid region ($x > 0$ within the toroid of radius r_t), $\theta(x)$ would be ideally described by

$$\cos\theta(x) = 1/\sqrt{1 + (x/r_t)^2} \tag{4}$$

for $x \geqslant 0$, while $\theta = 0$ for $x < 0$. A real situation with a steady variation of the magnetic-field curvature is described by a smoothly increasing function $\theta(x)$ between $x_{\min} < 0$ (beginning of significant field perturbation within the solenoid) and $x_{\max} > 0$ (point within the toroid where the ions cease to be overlapped with the electron beam). The correction to the rate coefficient is applied iteratively using the relation [45]

$$\alpha^{(i+1)}(E_d) = \alpha^{(0)}(E_d) - \frac{2}{L}\int_{x_{\min}}^{x_{\max}} \alpha^{(i)}(\tilde{E}_d(x, E_d))\, dx. \tag{5}$$

Here, the starting value of the iteration is obtained from Eq. (2) setting $L = L_{\mathrm{sol}} + 2x_{\min}$ (corresponding to the portion of the overlap length assumed to be exactly straight, i.e., where $\tilde{E}_d \equiv E_d$). The factor of 2 in Eq. (5) describes the two symmetrically arranged toroids. Using this basic approach, the corrections of the measured cross section for this effect are performed in slightly different ways in the three experiments, as explained below referring to the "toroidal correction."

(e) Correction of the experimental electron collision energies to account for changes due to the friction (or drag force) exerted by the electron on the ion beam. This interaction is able to change the ion-beam velocity, and is of particular importance when applying a voltage ramp, such as in the method used at CRYRING. Similarly, in the procedure applying voltage jumps, shifts of the ion velocity that smear the structure of the cross section may appear if the detuning energy is small. Generally, the friction can introduce uncertainties in the exact size of the detuning energy at $E_d \lesssim 10^{-3}$ eV.

(f) Considerations of field ionization of recombination products in the bending magnet after the electron cooler. If product atoms are formed in high Rydberg states (which becomes possible at collision energies above ~ 2 eV) this process may lead to an underestimation of the DR cross section. Table I shows the cutoff principal quantum number n_c for the three rings, as calculated from the motional electric field F

seen by the fast neutral fragments when passing the bending magnet. The cutoff n_c is determined as the smallest integer $>(16F)^{-1/4}$, with F in atomic units, corresponding to the saddle-point limit for field ionization [46]. The rather large values of n_c indicate that only small corrections should occur due to field ionization. Further discussion follows in Sec. IV.

C. Procedures of the individual experiments

1. ASTRID

Results reported here from ASTRID were obtained by chopping the electron-beam current on and off. DR events (appearing at full beam energy) and background events (H counts at 1/3 and D counts at 2/3 of the full beam energy) are collected simultaneously by feeding the detector signals into three single-channel analyzers (SCA). Their upper and lower discrimination levels are set by comparison with the complete pulse height spectrum recorded with a separate multichannel analyzer. The outputs of the SCA then enter a multichannel scaler (MCS) together with the digitized electron current.

The absolute value of the rate coefficient is obtained, for a fixed detuning velocity, by recording the DR signal, the electron and the ion currents simultaneously, as a function of the time after injection. Indeed, the ASTRID current transformer gives reliable values down to 50 nA, with an estimated uncertainty of 20% at this low value.

The analysis of the rate coefficient data at $\sim$0.3–3 eV, in particular, requires that the so-called toroidal correction be applied to account for the regions in the electron cooler where the electron beam is bent in to and out of the cooler (see Sec. II B). At ASTRID, results were corrected by using Eq. (3) with the idealized dependence of the magnetic field direction $\theta(x)$ of Eq. (4). The iterative procedure of Eq. (5) (using $x_{\min}=0$) was also compared to a different procedure making use of the fact that the DR rate coefficient becomes negligibly small at high electron energies. With this assumption, starting at such a high energy $E_d^{(n)}$ that the correction arising from detuning energies $\tilde{E}_d > E_d^{(n)}$ can be disregarded, the final corrected rate coefficients are obtained at all lower-energy points $E_d^{(i)} < E_d^{(n)}$ (i.e., for $E_d^{(i)}$ in descending order) directly as

$$\alpha(E_d^{(i)}) = \alpha^{(0)}(E_d^{(i)}) - \frac{2}{L}\int_{x_{\min}}^{x_{\max}} \alpha(\tilde{E}_d(x, E_d^{(i)}))dx, \qquad (6)$$

where the integral needs the corrected rate coefficient only at higher energies $\tilde{E}_d > E_d^{(i)}$ where it has already been determined. The results for $\alpha(E_d)$ obtained by the iteration according to Eq. (3) and the one-pass sequential calculation according to Eq. (6) were found to be the same.

2. CRYRING

For the present experiments in CRYRING, the electron cooler voltage was slowly ramped and the neutral particle count rates were recorded as a function of time during these ramps. (Previous experiments at CRYRING [28] used the jump method as also applied at TSR and ASTRID.) To help with determination of the energy scale, the electron energy was ramped to be symmetrical around the cooling energy. As in ASTRID, the DR and background count rates were monitored with two MCS cards. At CRYRING the absolute ion current is determined with an estimated accuracy of 20% using a current transformer, and the current and the beam lifetime are measured simultaneously. The proportionality factor $\zeta = R_D/I_i$ is determined by monitoring the background count rate R_D after a number of ion-beam decay times and by extrapolating the ion current measured at the beginning of the storage cycle to the time of the count rate measurement. In this process it is verified that the beam lifetimes from the current transformer and from the MCS are the same.

At CRYRING the space-charge correction to the electron energy is determined empirically. For this purpose, first the electron acceleration voltage U_c at cooling (i.e., at matched electron and ion velocities) energy is found by optimizing the strength of the DR signal itself. The velocity of the cooled ion beam, and hence the laboratory electron energy E_e in the overlap region, is established accurately by measuring the orbiting frequency of the ions and using pick-up devices in the ring to find the circumference of the ion orbit. The laboratory electron energy at cooling thus derived is compared to the corresponding cathode voltage in order to determine the amount of space charge in the electron beam, using the general expression for the space-charge correction,

$$E_e = eU_c - (I_e/ev_e)r_e mc^2[1-\lambda\sigma_{\mathrm{EII}}(v_e)][1+2\ln(b/a)]. \qquad (7)$$

Here, b is the inner diameter of the vacuum tube (the reference for ground potential), a is the diameter of the electron beam, and r_e is the classical electron radius; the factor $\lambda\sigma_{\mathrm{EII}}(v_e)$ corrects for the presence of positive ions in the electron beam and is proportional to the electron-impact ionization cross section $\sigma_{\mathrm{EII}}(v_e)$ of the residual gas. The electron velocity dependence of the terms in Eq. (7) is taken into account in deriving the space-charge correction at electron energies detuned from cooling, solving this equation iteratively for the given U_c and I_e. As hydrogen is the dominant component in the residual gas, the ionization cross section of H_2 is used for $\sigma_{\mathrm{EII}}(v_e)$ in Eq. (7).

The correction procedure for the toroid effects at CRYRING was reconsidered for this work, applying a dependence of the magnetic-field angle $\theta(x)$ [cf. Eq. (3)] as determined from magnetic-field measurements at $x > x_{\min} = -12.5$ cm. The field angle caused by the toroid exceeds a value of 0.2 mrad at $x > -11.5$ cm.

In the voltage ramp method, a correction of the collision energy scale for the drag force is necessary. With a linear ramp of the cooler voltage, the following formula corrects for the drag force:

$$dv_i/dt = (\eta/M)(L/C)F_z(t). \qquad (8)$$

The left-hand side dv_i/dt gives the variation of the ion velocity with time; M denotes the ion mass and $\eta = (dv_i/v_i)/(dp_i/p_i)$ describes the storage-ring dispersion properties (p_i being the ion momentum). $F_z(t)$ is the longitudinal component of the drag force which was taken from

experimentally verified theoretical expressions summarized in Ref. [36]. The magnitude of η for CRYRING can be found in Ref. [44].

3. TSR

The general procedure employed at TSR was similar to earlier DR measurements at this facility (see, for example, Ref. [47]). Data acquisition started after the injected ions had been phase-space cooled and was continued for 10–15 s, with a typical injection cycle being $\sim$20 s long. TSR used the voltage-jump method, and the electron acceleration voltage was switched every 25 ms between three values. The first value yielded the desired detuning energy E_d for the measurement. The second value was the cooling energy to maintain phase-space cooling of the ions. The third value was chosen to be at a fixed detuning energy of $E_{d,r}$ $=36.7$ eV (reference energy), where the DR cross section is nearly zero. The rate recorded in the ''reference'' phase represented the (small) capture background from residual-gas collisions and was subtracted from $R_{\mathrm{H+D}}(E_d)$ to yield the true recombination count rate $\overline{R}_{\mathrm{H+D}}(E_d)$. In the measurement with the narrow electron beam, the third step of the electron-energy cycle was chosen to be identical to the second one, as the true DR rate was much higher and subtraction of the capture background was unnecessary. Online normalization during the recombination measurement was performed using the D fragment count rate at the reference energy, $R_{\mathrm{D}}(E_{d,r})$. The normalization factor $\zeta=R_{\mathrm{D}}(E_{d,r})/I_i$ was determined separately, directly before and after the recombination measurement. The electric current probe cannot be used to monitor the ion current I_i continuously during the measurement because the count rates at the necessary ion current would destroy the detector. In the first step, the trigger rate R_{BPM} of the TSR beam profile monitor (BPM) [48] which counts ions produced in the residual gas by collisions with the circulating beam, was measured at low ion current simultaneously with $R_{\mathrm{D}}(E_{d,r})$; this yielded the constant λ_1 $=R_{\mathrm{D}}(E_{d,r})/R_{\mathrm{BPM}}$. Then the silicon detector was protected from the fragments, and the stored ion current was raised up to a maximum of 20 μA by stacking the ions in the ring, and $\lambda_2=R_{\mathrm{BPM}}/I_i$ was determined, finally yielding $\zeta=\lambda_1\lambda_2$. Two measurements of the cross section have been carried out for two different diameters of the electron beam to optimize for either the energy resolution or the signal count rate. The ''wide-beam'' measurement was put on an absolute scale using Eq. (2) and the ion current derived from the count rate $R_{\mathrm{D}}(E_{d,r})$ with help of the parameter ζ. The ''narrow-beam'' measurement was not absolutely calibrated, and an energy-averaged DR cross section was obtained via

$$\langle \sigma v\rangle/v_d = F\,\overline{R}_{\mathrm{H+D}}(E_d)/R_{\mathrm{H+D}}(E_d=0). \tag{9}$$

Here, $R_{\mathrm{H+D}}(E_d=0)$ represents the recombination rate measured when the electron-beam energy was cycled back after each data point to the cooling energy (i.e., detuning energy $E_d=0$). The overall normalization factor F was determined by forcing agreement with the wide-beam measurement at energies E_d between 5 and 12 eV.

As mentioned earlier, for the experiment at TSR the space-charge neutralization, arising from the accumulation of slow ions in the electron beam, is prevented by the use of clearing electrodes, in the downstream toroidal sections, which continuously remove the trapped slow ions. Furthermore, at TSR, the space-charge conditions in the cooler were verified in several earlier experiments on electron cooling and on dielectronic recombination of atomic ions. Details regarding the determination of the experimental energy scale in the TSR recombination experiments have been described elsewhere [43].

The electron-beam diameter and the transverse electron temperature in the interaction region are determined from the magnetic expansion of the electron beam. This expansion is given by the magnetic-field strength in the electron gun. Two different settings were applied in the TSR measurements (see Table I). The wide-beam measurement offered very good energy resolution at near-zero energies, while the narrow-beam measurement had the advantage of a much higher electron density (2×10^7 cm^{-3}), providing higher particle rates for measurements at low cross sections. Furthermore, the overlap length in the bends was reduced from 41 cm with the wide beam to 25 cm with the narrow beam and the excess energies encountered in the bending regions became smaller. In the following discussion of the results, the TSR data shown in the comparison are from the wide-beam measurement (high-energy resolution) at $E_d<0.31$ eV and from the narrow-beam measurement (high-electron density) at E_d >0.31 eV. These two settings allowed an empirical check to be performed on the correction procedure for the bending regions according to Eq. (5) by comparing the final results for both measuring modes. All TSR data were corrected for the contributions from the bending regions of the electron beam using a function $\tilde{E}_d(x,E_d)$ (see Sec. II C 1) according to measured magnetic fields at $x>x_{\mathrm{min}}=-15.0$ cm, which coincides with the range where the field angle caused by the toroid exceeds a value of 0.2 mrad.

III. RESULTS

A. DR cross section

The absolute experimental cross sections measured as a function of the detuning energy E_d between the electron and the HD^+ ion beam are shown in Fig. 2. For reasons of clarity, the curves of CRYRING and TSR have been shifted up by one and two decades, respectively. Note the large dynamic range of these measurements, both the energy and the cross section spanning many decades; detailed comparisons between the datasets will be given step by step in the following. Differences between the measurements due to the individual experimental parameters are expected to occur if the detuning energies become similar to or less than the electron temperature ($E_d \lesssim kT_{e\perp}$, cf. Table I). The experimental cross section $\langle \sigma v\rangle/v_d$ then significantly differs from the true cross section $\sigma(E)$ because of the averaging over the finite collision energy resolution. This leads to the suppression of many structures in the cross section below $\sim$0.1 eV for the results from ASTRID which, owing to the lower magnetic expan-

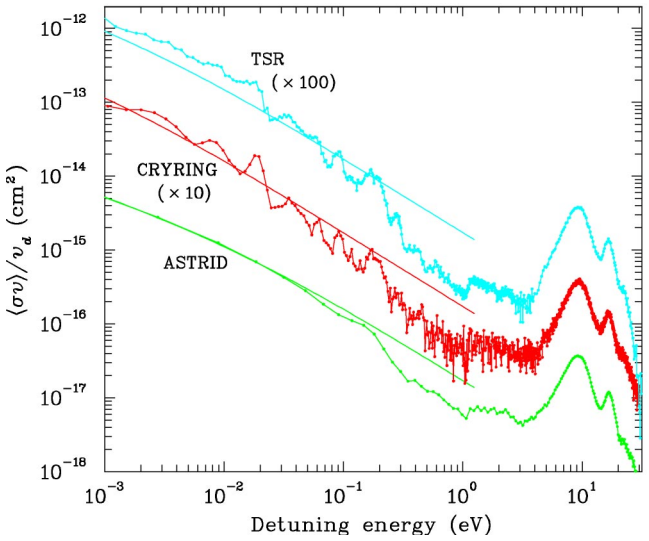

FIG. 2. (Color online) Overview of the DR cross sections $\langle \sigma v \rangle / v_d$ measured at the three storage rings as a function of the detuning energy E_d. The curves have been shifted with respect to each other for clarity as indicated. All smooth curves represent the folded model cross section $\sigma(E) = A/E$ fitted to the ASTRID data at low energy.

sion available, used a much higher transverse electron temperature than CRYRING and TSR. The lowest data points from ASTRID can be fitted very well by the folded cross section $\langle \sigma v \rangle / v_d$ obtained for a smooth model cross section $\sigma(E) = A/E$ and the experimental electron velocity distribution of Eq. (1), using the ASTRID electron temperatures from Table I. The constant A of the model cross section is determined from a fit to the ASTRID data to be 1.73×10^{-17} cm^2 eV within a normalization error of $\pm 20\%$ (see Sec. II B). To guide the eye, the folded model cross sections calculated with the same constant A, but with the respective electron temperatures of the other experiments, are also shown for CRYRING and TSR. These convoluted $1/E$ cross sections pass through the resolved low-energy structures ($E_d \lesssim 0.1$ eV) in a rather good approximation.

Considering that the rough overall variation of the DR cross section follows a $1/E$ scaling, we present the data also as the scaled cross section $E_d \langle \sigma v \rangle / v_d$ versus the detuning energy E_d. Indeed, Fig. 3 much better shows the strong variations of the DR rate at low electron energies. In the high-energy region ($E_d > 5$ eV), excellent agreement between the three independently calibrated measurements is found; the differences among them are below $\pm 10\%$. The low-energy structures are roughly consistent with each other, but some quantitative differences also occur, which will be analyzed below. In the following presentation we compare the results in detail for three different energy regions: (a) the low-energy region below 400 meV, (b) the valley region between 100 meV and 2 eV, where the cross section is minimal, and (c) the high-energy peaks above 2 eV.

We begin by the low-energy region. Figure 4 shows a comparison between 0.1 meV and 400 meV, presenting the unscaled experimental cross sections. Here the differences in collision energy resolution at the three rings must be taken

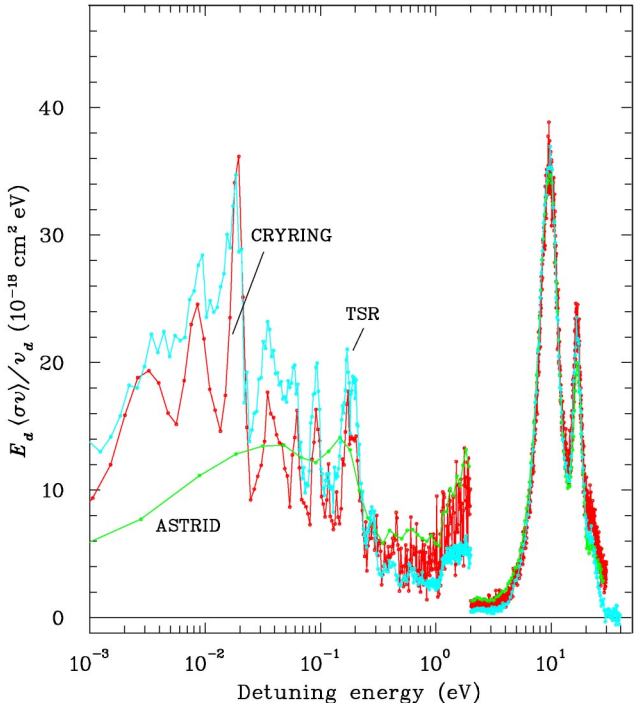

FIG. 3. (Color online) Overview of the DR cross sections, presenting the scaled DR cross section $E_d \langle \sigma v \rangle / v_d$ from the three rings. For the energy values above 2 eV, the scaled DR has been multiplied by 0.1.

into account in the comparison. Considering the electron temperatures of Table I, the lower observed cross section at ASTRID below ~ 20 meV as compared to CRYRING and TSR is clearly caused by the lower resolution of this arrangement. The CRYRING and TSR data show relatively sharp features (see also Fig. 3); note the agreement in the positions and magnitude of the resonance structures, for example, near 8 ± 1 meV and 15 ± 2 meV. CRYRING shows an additional modulation of the cross section at about 4 ± 1 meV, which is

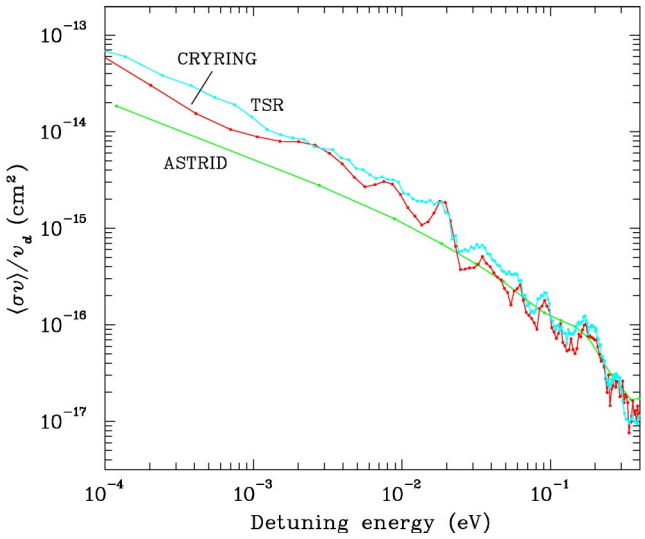

FIG. 4. (Color online) Comparison of the measured DR cross sections in the low-energy region.

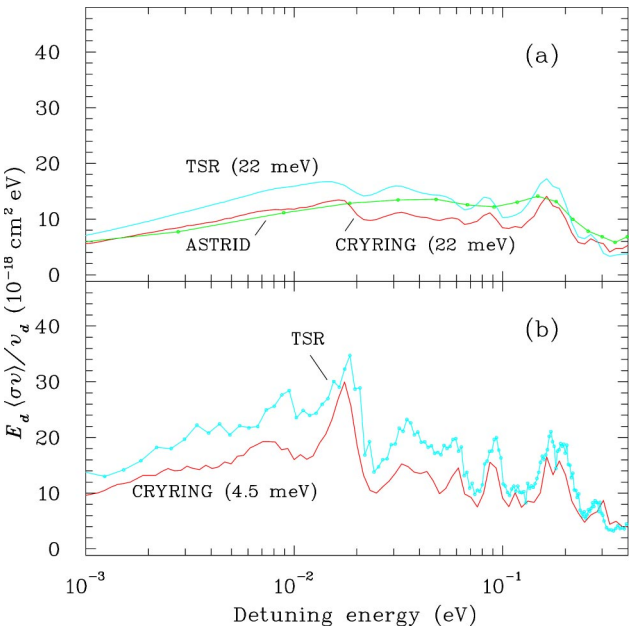

FIG. 5. (Color online) Comparison of the low-energy DR cross sections measured at ASTRID (a) and at TSR (b) with folded data from the other experiments using lower energy resolution. Curves for folded data are marked by the estimated final transverse electron temperatures obtained after the folding (see text).

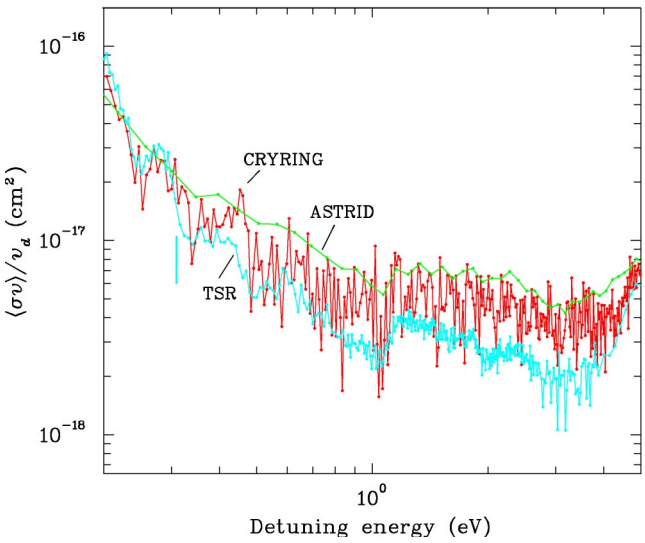

FIG. 6. (Color online) DR cross sections measured at intermediate energies (0.2–5 eV). The mark near the TSR data indicates the limit between the energy ranges where for this facility data from the wide-electron beam (detuning energy $E_d<0.22$ eV) and the narrow-electron beam are displayed.

absent in the TSR data. A higher-lying structure at ~150–200 meV appears not only for TSR and CRYRING but also in the ASTRID data. In Fig. 5(a) convoluted data from CRYRING and TSR are compared with the ASTRID dataset. The convolutions were chosen to obtain the final transverse temperature of the ASTRID measurement; as for Maxwellian convolutions the temperatures are additive, the transverse temperatures for the additional convolutions were chosen to be 20 meV and 17.5 meV for the CRYRING and the TSR data, respectively, to simulate a total transverse temperature of 22 meV in both cases. The sizes of the two artificially convoluted cross sections agree reasonably well with the ASTRID data. However, it is seen that the peak structure at ~150–200 meV even after the convolution procedures is still more narrow at TSR and CRYRING than at ASTRID; this may indicate that the transverse temperature for ASTRID is underestimated significantly. It is also seen that the convoluted TSR and CRYRING cross sections agree well in their structure, while the TSR cross section is substantially higher than that of CRYRING, the difference reaching up to 40%.

In Fig. 5(b) the CRYRING data were convoluted using a transverse temperature of 2.5 meV, which should yield the temperature of 4.5 meV expected for the TSR measurement, and compared to those data. This flattens out the modulation at ~4 meV and broadens the peaks at 8 and 15 meV as well as higher-lying structures up to ~50 meV in the CRYRING data, further improving the agreement between the shapes of the two cross sections, which reveal essentially the same fine structure. Also here, the TSR cross section is significantly larger than that of CRYRING with differences ranging up to 40% below 0.1 eV.

Next, we compare the valley region of the cross section between 0.2 eV and 2 eV, i.e., region (b). The cross sections in this region, obtained from the three rings, are shown in Fig. 6. The DR rate is much smaller than at lower and also at higher energies, so that long measuring times are required to obtain sufficiently low statistical scattering. All three data sets are consistent regarding the overall shape of the cross section and, more or less clearly, show a thresholdlike behavior in the cross section at a collision energy of ~1.1 eV. The group at TSR has remeasured this part of the spectrum and found that the cross section reveals characteristic structure related to the opening of new dissociation limits [29], of which the lowest one, at 1.1 eV, corresponds to the opening of the channel with one of the hydrogen atoms excited to $n=3$.

The presence of the strong and wide high-energy resonances adjacent to the valley region can cause significant effects in the measured rates from the toroid regions of the electron cooler, where the ions interact with electrons of higher energies (see Sec. II B). The size of the correction is essentially determined by the length over which the shifted relative energy $\tilde{E}_d(x,E_d)$ [see Eq. (3)] lies in the range of the high-energy resonance and has to be estimated with high accuracy if the recombination rate at the measurement energy E_d itself is small. For the TSR data, the size of the toroid effect and its correction are illustrated in Fig. 7. The uncorrected data obtained with the wide and the narrow electron beam (cf. Table I) differ considerably from each other [Fig. 7(a)]. This can be well understood from the different lengths over which the ions see misaligned electrons ($x_{\max}=19$ cm for the wide and $x_{\max}=10.5$ cm for the narrow beam) and the corresponding large difference in the maximum excess center-of-mass energy (22 eV for the wide beam but only ~9 eV for the narrow beam). Hence, the uncor-

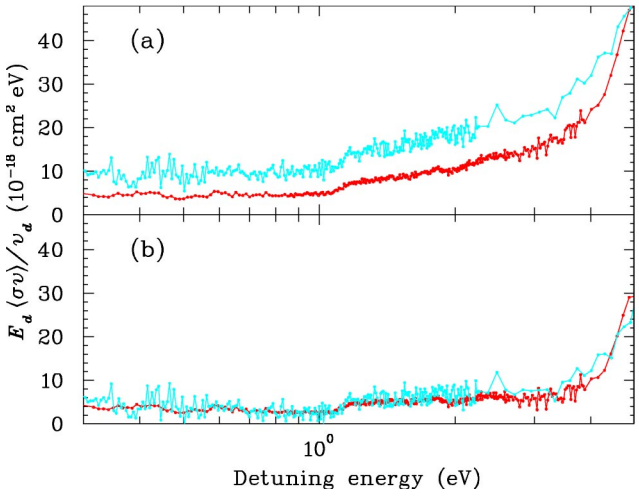

FIG. 7. (Color online) Scaled DR cross section $E_d\langle\sigma v\rangle/v_d$ measured at the TSR (a) before and (b) after the toroid correction. The wide- and the narrow-beam data are shown as lighter and darker traces, respectively. (Online colors: cyan and red, respectively.)

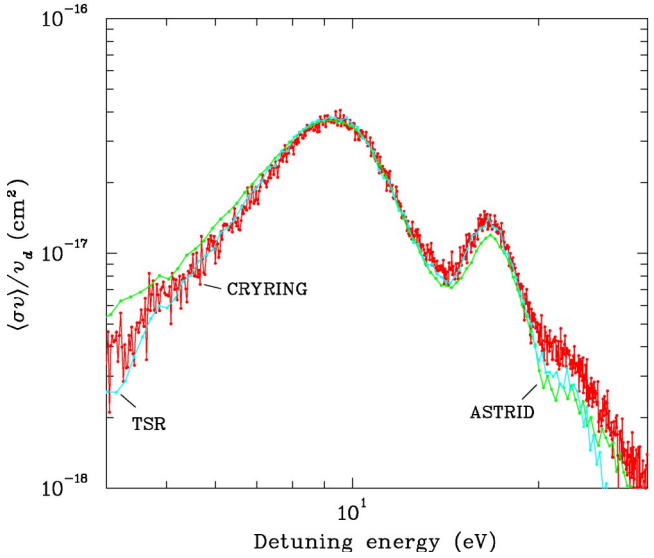

FIG. 8. (Color online) DR cross sections $\langle\sigma v\rangle/v_d$ measured at high energies (4–30 eV).

rected data differ by up to 100% at 0.3–1.5 eV. The final results [Fig. 7(b)] are consistent with each other, although very different toroid corrections are subtracted (up to 70% for the wide, but less than 35% for the narrow beam). This consistency for the two beam geometries gives a strong support for the accuracy of the toroidal correction in the TSR measurements.

Nevertheless the final results from the other experiments somewhat exceed the TSR result. For ASTRID, using an idealized field geometry [Eq. (4)] in the correction procedure, the size of the toroid correction may be underestimated explaining the high level of these data. For CRYRING, use of measured instead of estimated data for the geometry function $\theta(x)$ brought a significant reduction in the final result, but not down to the level of TSR. Altogether, in spite of careful cross checks of the toroid correction procedure within and between the different experiments, significant unexplained discrepancies remain in the final result for the absolute size DR cross section in the valley region (see Fig. 6). This can be relevant for a detailed comparison with theoretical calculations and for the thermal DR rate coefficients in some ranges of higher temperature (>1000 K), but should be of less influence for DR rate coefficients in low-temperature environments.

For region (c), comprising the high-energy peaks, a comparison between the DR data from the three facilities is shown in Fig. 8. The increase of the cross section in this region is connected with the occurrence of a large Franck-Condon overlap between the HD^+ vibrational ground state and the higher members of the doubly excited Q_1 series [49] that also includes the $(2p\sigma_u)^2\,{}^1\Sigma_g^+$ state mainly responsible for the low-energy DR. The Q_1 states dissociate to various combinations of $H(nl)+D(1s)$ and $H(1s)+D(nl)$ products. The second high-energy peak at 16 eV is due to formation of doubly excited Q_2 states dissociating to $H(nl)+D(2l')$ or $H(2l')+D(nl)$ atoms. In the high-energy region the data from the three experiments agree well within the error limits of 20% estimated for the independent absolute normalizations. For the DR cross section at the first high-energy peak the experiments agree even within their statistical errors ($\pm 0.2\times 10^{-17}$ cm^2). The joint result, including the 20% overall normalization error, is $(3.5\pm 0.7)\times 10^{-17}$ cm^2; the peak position is found at 9.8 ± 0.2 eV. For the second high-energy peak the joint result is $(1.3\pm 0.3)\times 10^{-17}$ cm^2 at 16.6 ± 0.2 eV.

B. Thermal rate coefficients

The measured energy dependent cross sections can be used to derive thermal rate coefficients for the DR of HD^+ by folding them with an isotropic Maxwellian energy distribution. For a temperature T of an isotropic electron gas the thermal rate coefficient $\alpha_{\rm th}(T)$ is related to the cross section $\sigma(E)$ by

$$\alpha_{\rm th}(T)=\frac{4}{\sqrt{2\pi mkT}}\int_0^\infty E\sigma(E)e^{-E/kT}d\left(\frac{E}{kT}\right). \qquad (10)$$

In deriving thermal rate coefficients from the present experimental cross sections, the following aspects must be taken into account. First, the measured cross sections actually represent the folded quantity $\langle\sigma v\rangle/v_d$ (see Sec. II B) and for low temperatures the experimental electron velocity distribution [Eq. (1) with the respective experimental parameters from Table I] will have an effect if measured cross sections are directly inserted into Eq. (10). Second, the thermal rate coefficients we obtain here hold for HD^+ ions with a rovibrational excitation that does not follow the electron temperature T as would be the case in a plasma situation. Thus, the electron energy range scanned in the present experiments would allow thermal rate coefficients to be derived for electron temperatures up to 10^4 K or more, but such temperatures in a plasma situation would correspond to a high degree of vibrational excitation, while the present data are obtained

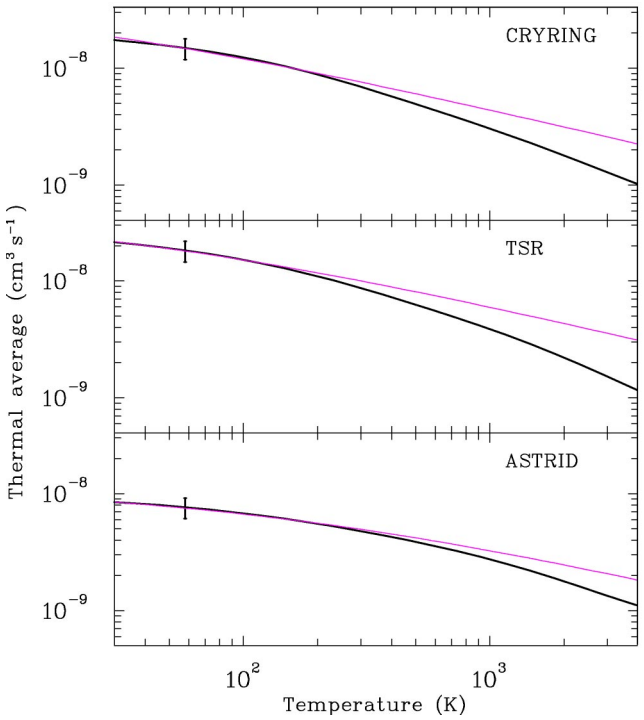

FIG. 9. (Color online) Thermal averages α_{av}, shown as functions of the isotropic Maxwellian electron temperature T, for the measured DR cross sections from the three experiments (black lines) and for model cross sections $\sigma(E)=A/E$ folded with the respective experimental electron velocity distributions (gray lines; online color: magenta). The model cross sections were scaled to fit the experimental thermal averages for low T. The error bars indicate the overall experimental normalization errors.

for vibrationally cold HD^+ ions. The rotational temperature of the stored $HD^+(v=0)$ ions is not well known, but was estimated to ~ 500 K from earlier DR fragment imaging data [33].

We have derived thermal averages defined, in analogy to α_{th}, by

$$\alpha_{\mathrm{av}}(T)=\frac{4}{\sqrt{2\pi mkT}}\int_0^\infty E_d\frac{\alpha(E_d)}{v_d}e^{-E_d/kT}d\left(\frac{E_d}{kT}\right) \quad (11)$$

from the measured cross sections $\alpha(E_d)/v_d=\langle\sigma v\rangle/v_d$ of the three experiments.

The averages α_{av} are shown in Fig. 9. These can be interpreted directly as thermal rate coefficients at $T\gtrsim 300$ K for CRYRING, $T\gtrsim 600$ K for TSR, and $T\gtrsim 3000$ K for ASTRID; above the given limits, the errors introduced by neglecting the experimental energy resolution are $<10\%$ (as was verified for a $1/E$ model cross section). In order to quantify the thermal rate coefficient at lower temperatures, we compare the experimental averages α_{av} with calculated averages obtained using Eq. (11) for a model cross section $\sigma(E)=A/E$ and for the specific experimental electron temperatures (Table I). As seen in Fig. 9, these calculated curves for an appropriate choice of A yield a good representation of the experimental averages at electron temperatures of the order of 100 K. The fitted constants A can be used to obtain thermal rate coefficients from Eq. (10) using the A/E model cross sections. Taking into account the estimated normalization errors, the low-temperature thermal rate coefficients obtained by this method are $\alpha_{\mathrm{th}}=7.2(1.5)\times10^{-9}$ cm^3 s$^{-1}\times(300\,\mathrm{K}/T)^{1/2}$ for ASTRID, $\alpha_{\mathrm{th}}=8.3(1.7)\times10^{-9}$ cm^3 s$^{-1}\times(300\,\mathrm{K}/T)^{1/2}$ for CRYRING, and $\alpha_{\mathrm{th}}=11.7(2.4)\times10^{-9}$ cm^3 s$^{-1}\times(300\,\mathrm{K}/T)^{1/2}$ for TSR. The cross-section constant A implied by the ASTRID result is identical to the one used for the smooth curves in Fig. 2.

The agreement between the three experiments on the low-energy rate coefficient is not as good as on the high-energy cross section (Fig. 8); however, the results given above are still compatible within the estimated errors. Hence, it appears reasonable to extract the average of $\alpha_{\mathrm{th}}=(9\pm2)\times10^{-9}$ cm^3 s$^{-1}\times(300\,\mathrm{K}/T)^{1/2}$ as a joint result for the thermal DR rate coefficient of HD^+ ions in a temperature range of $\sim$50–300 K.

IV. DISCUSSION

All three heavy-ion storage rings have evolved instrumentally in the last few years. The mere fact that experiments have been performed on the same molecular systems at different facilities has significantly increased the awareness on experimental details. For example, toroidal corrections were initially not applied to some data [28,47]. Beam drag, which may shift resonances present at low energies to higher energies, has been taken care of. Space-charge effects, which affect the determination of the absolute collision energy, have been treated in much more detail.

Two earlier absolute measurements of the DR cross section of HD^+ have been published [26,28] and further data, obtained with a novel superconducting quantum interference device ion current sensor at TARNII, were reported recently [50]. The previous measurements raised discussion [7,26] because of some discrepancy regarding the height of the high-energy peak near 9 eV, CRYRING [28] yielded a cross section maximum of 3.0×10^{-17} cm^2, while ASTRID [26] (as also the more recent data [50] from TARNII) yielded 5.0×10^{-17} cm^2. The present three storage-ring measurements (Fig. 8) jointly give a peak height of $(3.5\pm0.7)\times10^{-17}$ cm^2, closer to the lower one of the previous results, and a peak position of 9.8 ± 0.2 eV. Theoretical values for the height and the position of the high-energy peak, taken from recent calculations for $HD^+(v=0)$ ions, are 3.9×10^{-17} cm^2 at 9.0 eV (Fig. 9 of Ref. [7]) as well as 4.8×10^{-17} cm^2 at 9.4 eV (Fig. 6(a) of Ref. [51]). Regarding the peak height, our data are better reproduced by the calculations of Ref. [7]. The data also indicate a slightly higher peak position than both calculations. The second high-energy peak has found less theoretical attention and is not discussed in more detail here.

Among the possible processes that could affect the measured signal at elevated collision energies the population of high-Rydberg atomic final states has been discussed above (Sec. II B). Mitchell and co-workers have observed Rydberg stripping to be important in a single-pass experiment involving highly vibrationally excited H_2^+ [23,24]. Calculations [51] indicate that for $HD^+(v=0)$ ions the partial DR cross

section at the high-energy peak for $n \geqslant 6$ final states is $\sim 1 \times 10^{-17}$ cm^2 ($\sim 20\%$ of the total); similarly, fragment branching-ratio measurements [52] performed for $n \geqslant 4$ at $E_d = 9.2$ eV at TSR yielded $(28 \pm 7)\%$. From these results, a reasonable upper limit on the reduction of the DR signal by field ionization, considering $n_c \sim 10$ (see Table I) may be located at roughly 10%; such a shift would bring the theoretical predictions mentioned above in better agreement with experiment. The earlier experiment at CRYRING [28] was performed using an ion-beam energy of 18 MeV (against 3 MeV in the present experiment); the difference in ion energy shifted the field ionization limit down to $n_c = 6$ for the earlier experiment and may be responsible for the somewhat smaller high-energy peak in the DR cross section measured previously at CRYRING.

The occurrence of ion-pair formation as an extra fragment channel not detected in the present experiments would modify the total $HD^+ + e^-$ neutralization rate at a cross section level of at most 3×10^{-19} cm^2, as known from dedicated studies of the ion-pair formation process [53]. Modulations of about this size near the ion-pair formation threshold at ~ 2 eV were in fact observed in the HD^+ DR cross section and ascribed to this process [29]. On the 9 eV peak in the DR cross section, ion-pair formation should be negligible in comparison to the neutral product channels.

Towards lower electron energies, the earlier as well as the present measurements unanimously indicate a DR cross section close to 1.0×10^{-16} cm^2 at the highest point of the structure appearing near 0.15 eV (see Fig. 4). In refined theoretical calculations [6,7], which include rotational effects, the energy dependence of the cross section is well reproduced and a size of $\sim 2.0 \times 10^{-16}$ cm^2 (Fig. 3 of Ref. [6]) and $\sim 1.5 \times 10^{-16}$ cm^2 (Fig. 10 of Ref. [7]) can be extracted. These predictions both exceed the experimental result by more than its 20% estimated uncertainty.

The shape of the low-energy structures in the cross section, down to ~ 0.01 eV, is consistent among the present measurements (see Figs. 4 and 5) as well as with other high-resolution data [6,7,51]. With regard to the overall size of the cross section at ~ 0.01–0.1 eV and its trend towards even lower energy, the deviations between the individual experiments are still rather large, even considering the different experimental resolutions (cf. Fig. 5). Nevertheless, the present measurements yield thermal rate coefficients for the DR of $HD^+(v=0)$ ions which agree within the estimated normalization errors of $\pm 20\%$. The joint result of $\alpha_{\mathrm{th}} = (9 \pm 2) \times 10^{-9}$ cm^3 s^{-1} at 300 K is rather well reproduced by the low-J ($J \leqslant 4$) theoretical thermal rate coefficients ($\sim 1.0 \times 10^{-8}$ cm^3 s^{-1} at 300 K) from Fig. 6(a) of Ref. [7]. Although, as mentioned in Sec. III B, the rotational temperature of the stored HD^+ ions is not well known, the estimated temperatures of the order of 300–800 K correspond to a dominant population in $J \leqslant 4$. Remarkably, the predicted thermal rate coefficients for higher-J levels [7] ($J = 5$–10) are larger by factors of 2–4; hence only the low-J theoretical results are in agreement with the present experiments. Furthermore, at temperatures $\lesssim 100$ K the calculated thermal rate coefficients for HD^+ [7] start to show a very strong dependence on J (variations over $> 10^2$ for $J = 0$–4). It cannot be excluded that some of the disagreement between the cross sections measured for very low electron energies at different experimental facilities might be caused by differences in the HD^+ rotational population distributions.

These measurements demonstrate that heavy-ion storage rings have a great potential in retrieving quantitative properties of dissociative recombination. The instrumental collision energy resolution is very high. The electron beam exceeds the size of the ion-beam significantly, which creates a very well defined overlap region. The time between injection of the ions and the data taking can be used to change and also to manipulate the ion beam population by selective excitation. For these experiments, radiative cooling of the HD^+ ions resulted in a well-defined $HD^+(v=0)$ ion beam.

The 20% error margin on the cross-section scale, estimated to account for the systematic uncertainties in the absolute current determination and in the geometry of the interaction region for the individual experiments, has been confirmed by this comparison. Critical electron energy regions where some disagreements are observed between different experimental setups are that of $E_d \lesssim 0.05$ eV, as discussed above, and the valley region of the cross section, $E_d \sim 0.4$–4 eV, where spurious signals stemming from the high-energy DR peak must be accounted for by the toroidal correction. Because of the arrangement of the molecular energy levels, DR studies on H_2^+ and its isotopomers are particularly sensitive to this type of experimental artifacts. By the proven correction procedure these artifacts can be expected to be eliminated even more efficiently in other molecular systems, which often have less accentuated high-energy DR peaks. Processes with a sharp energy threshold such as ion-pair formation and electron detachment from negative ions can give complementary information to further optimize the experimental correction procedure.

In conclusion, the present comparison of results from three different ion storage rings has yielded consolidated experimental information on the absolute DR cross section and on the thermal DR rate coefficient of $HD^+(v=0)$ ions, suitable for a detailed comparison with theoretical predictions. Satisfactory agreement between the individual experiments and with the calculations has been obtained for electron energies above ~ 0.01 eV. At lower energies, the influence of rotational excitations presents an interesting area of further investigations.

ACKNOWLEDGMENTS

We want to express our thanks to the accelerator scientists and the technical staff of the ion storage-ring facilities ASTRID, CRYRING, and TSR. For W.J.vdZ and R.T., this work is part of the research of the Stichting ''voor Fundamenteel Onderzoek der Materie'' and made possible by financial support from the Nederlandse Organisatie voor Wetenschappelijk Onderzoek. The work at ASTRID was supported by the Danish National Research Foundation through the Aarhus Center for Atomic Physics (ACAP). The work at TSR was partly funded by the German Federal Min-

ister for Education, Science, Research and Technology (BMBF) under Contract No. 06 HD 854 I, by the German Israel Foundation (GIF) under Contract No. I-0452-200.07/95, and by the German Federal Minister for Education, Science, Research and Technology (BMBF) within the framework of the German-Israeli Project Cooperation in Future-Oriented Topics (DIP). The present joint project is part of the research supported in the European Community's Research Training Networks Program under Contract No. HPRN-CT-2000-0142, ETR.

[1] D.R. Bates, Phys. Rev. **78**, 492 (1950).
[2] A. Sternberg and A. Dalgarno, Astrophys. J. **99**, 565 (1995).
[3] D. Kella, P.J. Johnson, H.B. Pedersen, L. Vejby-Christensen, and L.H. Andersen, Phys. Rev. Lett. **77**, 2432 (1996).
[4] D. Kella, L. Vejby-Christensen, P.J. Johnson, H.B. Pedersen, and L.H. Andersen, Science **276**, 1530 (1997); **277**, 167 (1997).
[5] R. Peverall *et al.*, Geophys. Res. Lett. **27**, 481 (2000).
[6] T. Tanabe *et al.*, Phys. Rev. Lett. **75**, 1066 (1995).
[7] I.F. Schneider, C. Strömholm, L. Carata, X. Urbain, M. Larsson, and A. Suzor-Weiner, J. Phys. B **30**, 2687 (1997).
[8] H. Takagi, in *Dissociative Recombination: Theory, Experiment and Application IV*, edited by M. Larsson, J.B.A. Mitchell, and I.F. Schneider (World Scientific, Singapore, 2000), p. 180.
[9] M.A. Biondi and S.C. Brown, Phys. Rev. **75**, 1700 (1949).
[10] N.G. Adams, in *Dissociative Recombination: Theory, Experiment and Applications*, edited by B.R. Rowe, J.B.A. Mitchell, and A. Canosa (Plenum, New York, 1993), p. 99.
[11] G.H. Dunn, B.V. Zyl, and R.N. Zare, Phys. Rev. Lett. **15**, 610 (1965).
[12] D. Auerbach, R. Cacak, R. Caudano, C.J. Keyser, T.D. Gaily, J.B.A. Mitchell, J.W. McGowan, and S.F.J. Wilk, J. Phys. B **10**, 3797 (1977).
[13] T. Tanabe *et al.*, Nucl. Instrum. Methods Phys. Res. A **307**, 7 (1991).
[14] S. Datz and M. Larsson, Phys. Scr. **46**, 343 (1992).
[15] T. Tanabe, I. Katayama, N. Inoue, K. Chida, Y. Arakaki, T. Watanabe, M. Yoshizawa, S. Ohtani, and K. Noda, Phys. Rev. Lett. **70**, 422 (1993).
[16] P. Forck, M. Grieser, D. Habs, A. Lampert, R. Repnow, D. Schwalm, A. Wolf, and D. Zajfman, Phys. Rev. Lett. **70**, 426 (1993).
[17] M. Larsson *et al.*, Phys. Rev. Lett. **70**, 430 (1993).
[18] S.P. Møller, in *Conference Record of the 1991 IEEE Particle Accelerator Conference*, edited by K. Berkner (IEEE, New York, 1991), p. 2811.
[19] K. Abrahamsson *et al.*, Nucl. Instrum. Methods Phys. Res. B **79**, 269 (1993).
[20] D. Krämer *et al.*, Nucl. Instrum. Methods Phys. Res. A **287**, 268 (1989).
[21] B. Peart and K. Dolder, J. Phys. B **6**, 359 (1973).
[22] R.A. Phaneuf, D.H. Crandall, and G.H. Dunn, Phys. Rev. A **11**, 528 (1975).
[23] H. Hus, F.B. Yousif, C. Noren, and J.B.A. Mitchell, Phys. Rev. Lett. **60**, 1006 (1988).
[24] P. van der Donk, F.B. Yousif, J.B.A. Mitchell, and A.P. Hickman, Phys. Rev. Lett. **67**, 42 (1991).
[25] P. Forck, M. Grieser, D. Habs, A. Lampert, R. Repnow, D. Schwalm, A. Wolf, and D. Zajfman, Nucl. Instrum. Methods Phys. Res. B **79**, 273 (1993).
[26] L.H. Andersen, P.J. Johnson, D. Kella, H.B. Pedersen, and L. Vejby-Christensen, Phys. Rev. A **55**, 2799 (1997).
[27] T. Tanabe *et al.*, Nucl. Instrum. Methods Phys. Res. A **441**, 326 (2000).
[28] C. Strömholm *et al.*, Phys. Rev. A **52**, R4320 (1995).
[29] M. Lange, J. Levin, G. Gwinner, U. Hechtfischer, L. Knoll, D. Schwalm, R. Wester, A. Wolf, X. Urbain, and D. Zajfman, Phys. Rev. Lett. **83**, 4979 (1999).
[30] H.T. Schmidt, L. Vejby-Christensen, H.B. Pedersen, D. Kella, N. Bjerre, and L.H. Andersen, J. Phys. B **29**, 2485 (1996).
[31] W.J. van der Zande, J. Semaniak, V. Zengin, G. Sundström, S. Rosén, C. Strömholm, S. Datz, H. Danared, and M. Larsson, Phys. Rev. A **54**, 5010 (1996).
[32] Z. Amitay *et al.*, Science **75**, 281 (1998).
[33] Z. Amitay *et al.*, Phys. Rev. A **60**, 3769 (1999).
[34] Z. Amitay, D. Zajfman, and P. Forck, Phys. Rev. A **50**, 2304 (1994).
[35] S. Krohn, Z. Amitay, A. Baer, D. Zajfman, M. Lange, L. Knoll, J. Levin, D. Schwalm, R. Wester, and A. Wolf, Phys. Rev. A **62**, 032713 (2000).
[36] H. Poth, Phys. Rep. **196**, 135 (1990).
[37] L.H. Andersen and J. Bolko, Phys. Rev. A **42**, 1184 (1990).
[38] H. Danared, Nucl. Instrum. Methods Phys. Res. A **391**, 24 (1997).
[39] G. Gwinner *et al.*, Phys. Rev. Lett. **84**, 4822 (2000).
[40] V.I. Kudelainen, V.A. Lebedev, I.N. Meshkov, V.V. Parkhomchuk, and B.N. Sukhina, Zh. Eksp. Teor. Fiz. **83**, 2056 (1982) [Sov. Phys. JETP **56**, 1191 (1982)].
[41] H. Danared *et al.*, Phys. Rev. Lett. **72**, 3775 (1994).
[42] S. Pastuszka *et al.*, Nucl. Instrum. Methods Phys. Res. A **369**, 11 (1996).
[43] G. Kilgus, D. Habs, D. Schwalm, A. Wolf, N.R. Badnell, and A. Müller, Phys. Rev. A **46**, 5730 (1992).
[44] D.R. DeWitt, R. Schuch, H. Gao, W. Zong, S. Asp, C. Biedermann, M.H. Chen, and N.R. Badnell, Phys. Rev. A **53**, 2327 (1996).
[45] A. Lampert, A. Wolf, D. Habs, J. Kenntner, G. Kilgus, D. Schwalm, M.S. Pindzola, and N.R. Badnell, Phys. Rev. A **53**, 1413 (1996).
[46] T.F. Gallagher, *Rydberg Atoms* (Cambridge University Press, Cambridge, 1994), p. 84.
[47] Z. Amitay, D. Zajfman, P. Forck, U. Hechtfischer, B. Seidel, M. Grieser, D. Habs, D. Schwalm, and A. Wolf, Phys. Rev. A **54**, 4032 (1996).
[48] B. Hochadel, F. Albrecht, M. Grieser, D. Habs, D. Schwalm, E. Szmola, and A. Wolf, Nucl. Instrum. Methods Phys. Res. A **343**, 401 (1994).

[49] S.L. Guberman, J. Chem. Phys. **78**, 1404 (1983).
[50] T. Tanabe *et al.*, in *Dissociative Recombination: Theory, Experiment and Application IV* (Ref. [8]), p. 170.
[51] H. Takagi, Phys. Scr. **T96**, 52 (2002).
[52] D. Zajfman, Z. Amitay, C. Broude, P. Forck, B. Seidel, M. Grieser, D. Habs, D. Schwalm, and A. Wolf, Phys. Rev. Lett. **75**, 814 (1995).
[53] A. Larson *et al.*, Phys. Rev. A **62**, 042707 (2000).